ELSEVIER

Physica D 119 (1998) 4–21

PHYSICA D

Localization in a coupled standard map lattice

M. Abel [a,*], S. Flach [b], A. Pikovsky [a]

[a] *Institute for Theoretical Physics and Astrophysics, University of Potsdam, Am Neuen Palais, PF 601553, D-14415, Potsdam, Germany*
[b] *Max-Planck-Institute for the Physics of Complex Systems, Nöthnitzer Str. 38, 01187 Dresden, Germany*

Received 15 May 1997; received in revised form 6 November 1997
Communicated by F.H. Busse

Abstract

We study spatially localized excitations in a lattice of coupled standard maps. Time-periodic solutions (breathers) exist in a range of coupling that is shown to shrink as the period grows to infinity, thus excluding the possibility of time-quasiperiodic breathers. The evolution of initially localized chaotic and quasiperiodic states in a lattice is studied numerically. Chaos is demonstrated to spread slowly along the lattice, with the globally chaotic regime appearing as an eventually statistically stationary state. A quasiperiodic initial state has extremely large life time for small couplings, and for large couplings evolves slowly into global chaos. © 1998 Elsevier Science B.V.

1. Introduction

There are two main mechanisms for the existence of localized excitations in conservative spatially extended systems. [1] In integrable systems such excitations appear as solitons [1], they survive at collisions and have many other particle-like properties. However, integrable systems are non-generic: even a small perturbation spoils integrability. Recently, another mechanism for the existence of localized excitations in rather general non-integrable systems has been proposed with the only restriction that the system should be discrete in space. Such localized excitations are called breathers [2,3].

Starting from the work of Takeno and Sievers [4–7] the investigation of localized excitations in discrete lattices became a topic of broad interest. Breathers have been reported to exist in lattices of the Fermi–Pasta–Ulam type as well as in Klein–Gordon type chains [8–10]. Physically, the existence of breathers can be understood from the properties of linear perturbations in the lattice [11]. Propagating waves have frequencies restricted to finite bands. Thus, if local oscillations on one lattice site have the property that all harmonics of this frequency lie outside these bands, these oscillations will not generate linear waves and the state can be localized. An explanation of this

* Corresponding author. Tel.: (49-331)-977-1604; fax: (49-331)-977-1142; e-mail: markus@agnld.uni-potsdam.de.

[1] Hereafter we define a localized solution as a state at a given time, which has the following spatial structure: for distances large compared to some extension of a central part, the state asymptotically tends to one and the same ground state, no matter what spatial direction is choosen. Thus we exclude especially kink-type solutions from further consideration.

PII S0167-2789(98)00060-8

behaviour as tangent bifurcation from the band edge was given in [12]. This argument works also in any spatial dimension [13].

A rigorous proof for the existence of breathers for a wide class of nonlinear lattices was given by MacKay and Aubry [14] using the concept of anti-integrability [15]. It was shown that under certain assumptions systems with general nonlinear on-site potentials posses breathers as exact solutions. The stability of these solutions has been studied in numerous publications [2,16–23]. An alternative approach was used in [24,25] where the existence of localized excitations was investigated by means of a mapping. Notice that in all these cases exact breather solutions, periodic in time are investigated.

The problem of existence of non-periodic breathers is not completely solved. There are arguments that quasiperiodic and chaotic breathers do not exist [24]. On the other hand, a perturbation of a stable periodic motion in a high-dimensional Hamiltonian system typically produces quasiperiodic motion, and therefore one can expect that quasiperiodic excitations exist at least as metastable states [22]. Moreover, quasiperiodic breathers were shown to exist in systems with additional symmetries like the discrete nonlinear Schrödinger equation [26,27]. The reason is a generalized formulation of the non-resonance condition as indicated in [28].

The main aim of this paper is to study the dynamics of quasiperiodic and chaotic "almost-breathers". To this end we have to deal with nonlinear lattices having non-trivial on-site dynamics, and we take a lattice of coupled standard maps [29,30] as a model. Different systems of coupled symplectic maps have been considered in [31–35]. In these papers mainly properties of the Arnol'd diffusion have been studied.

For periodic excitations there is an almost complete analogy to already considered models of coupled oscillators, and the localization properties can be understood to a large amount with the help of the analysis of the linearized problem. Additionally, considering larger and larger periods we can approach a quasiperiodic limit and study, what happens to the breathers in this case. To consider exact periodic and quasiperiodic states we rely mainly on direct simulations of the lattice dynamics. To investigate localized initial conditions, we start with a state where the first standard mapping is in a quasiperiodic or chaotic state, and other mappings are at rest and follow the evolution of this initially localized state in time. Our main results here are characterization of the spreading of perturbations in dependence on the excited state and the coupling.

The paper is organized as follows. In Section 2 we introduce the lattice of coupled symplectic maps and discuss in Section 3 its linear properties. In Sections 4 and 5 localized periodic states are analysed. Time evolution of initially localized quasiperiodic and chaotic states is described in Section 6.

2. The model

We consider a periodically kicked rotator described by the Hamiltonian

$$= \frac{2}{2} \quad {}_1(t)\cos \ , \tag{1}$$

where

$${}_1(t) = \sum_{n=-} \quad (t - n \ ) \tag{2}$$

By defining $({}_n, {}_n) = \lim {}_0 \ (\ (n \ - \ ), \ (n \ - \ ))$ as the values of (t) and (t) just before the nth kick and solving Hamilton's equations of motion between and during the kick, one obtains a discrete-time mapping:

$$ {}_{n\,1} \ = \ {}_n \quad \sin \ {}_n \ , \qquad {}_{n\,1} \ = \ {}_n \quad {}_{n\,1} \tag{3}$$

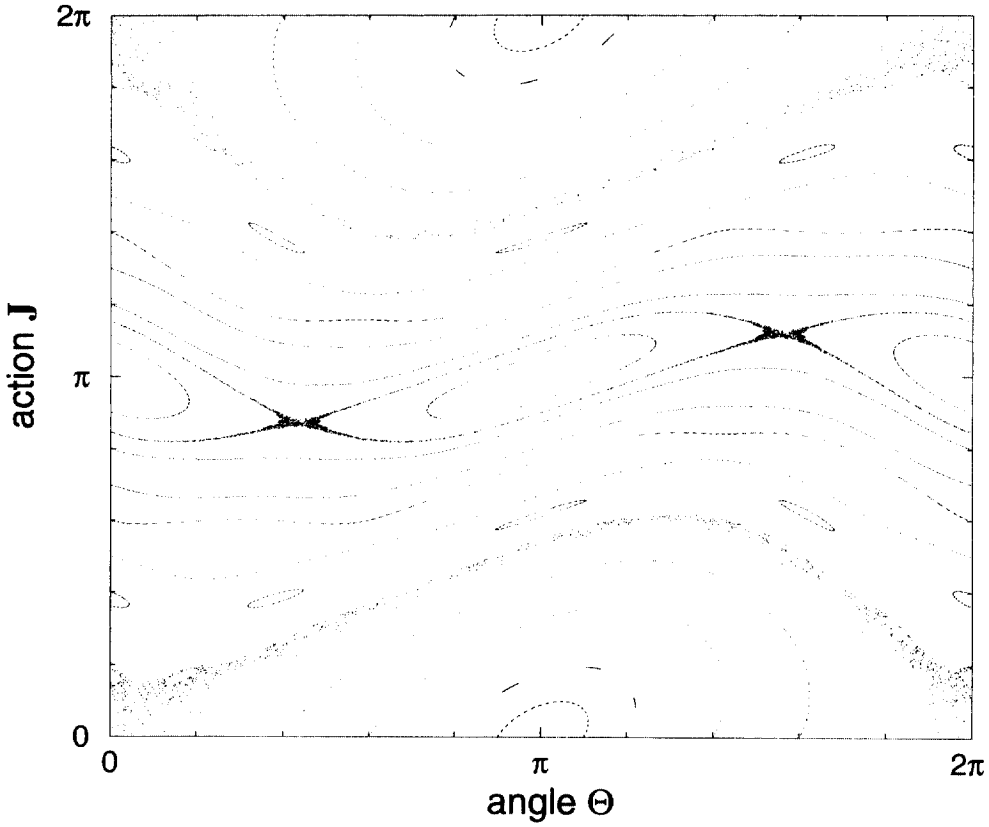

Fig. 1. The standard map with = 0 8 for a set of representative initial conditions.

This mapping is called the standard or Chirikov–Taylor mapping and is accepted as a characteristic example for Hamiltonian dynamics and Hamiltonian chaos [30,36]. The phase space can be considered as a whole phase plane, or, due to 2 -periodicity in and . as a torus 0 2 , 0 2 . The only parameter in these equations is the nonlinearity parameter . In the case of vanishing one has the regular motion of the rotator, for very large one has chaos and global diffusion in the whole phase space. For intermediate , i.e. = O(1), one typically observes, depending on the initial conditions, three different regimes (see Fig. 1):

- regime I: periodic orbits (stable or unstable);
- regime II: quasiperiodic motion which can be librational (around the periodic orbits) or rotational (on a KAM-curve);
- regime III: chaotic motion; it is restricted to isolated regions in the phase space, the largest one of these regions is the primary stochastic layer around the period-one fixed point.

Below we restrict our analysis to a moderate nonlinearity value = 0 8, since in this case all major regimes are present and clearly visible (Fig. 1). If we extend the system from one driven rotator to a system of coupled driven rotators, we have to add a coupling term to the equations of motion. To obtain a mapping in a compact form, it is convenient to consider the coupling also modulated with the sequence of -kicks (2). Although such a model does not directly correspond to a usual experimental set-up (a system of mechanical pendula fixed on a common bar, or a Josephson-junctions ladder [37,38]), we can suggest a possible realization for such a discrete coupling: One can imagine an array of pendula with coils on them. If a short pulse of current is passed through the coils, an interaction

force between the pendula will act during a short time and can be approximated with a -function. In the literature there are examples of global [33,39,40] and local [32,34] coupling. We consider a local, nearest-neighbour coupling: the Hamiltonian

$$= \sum_{=1} \frac{( )^2}{2} \quad {}_1(t) \sum_{=1} \cos \quad {}_1(t) \sum_{=1}^{-1} \cos({}^{1} -) \tag{4}$$

leads to the mapping

$$\begin{aligned} {}_{n\,1} &= {}_n \quad \sin {}_n - \sin({}_n{}^{1} - {}_n) \quad \sin({}_n - {}_n{}^{-1}), \\ {}_{n\,1} &= {}_n \quad {}_{n\,1} \end{aligned} \tag{5}$$

with the boundary conditions ${}^{0} = {}^{1}$ and ${}^{1} = \quad .$

3. Linear perturbations in the lattice

Consider the dynamics of linear perturbations around the stable fixed point $= 0, \quad = \quad .$ Linearizing (5) we get

$${}_{n\,1} = {}_n - \quad {}_n - ({}_n{}^{1} - 2 \, {}_n \quad {}_n{}^{-1}), \tag{6}$$

$${}_{n\,1} = {}_n \quad {}_{n\,1} \tag{7}$$

We can rewrite this system as a single equation

$${}_{n\,1} - 2 \, {}_n \quad {}_{n-1} = - \quad {}_n - ({}_n{}^{1} - 2 \, {}_n \quad {}_n{}^{-1}) \tag{8}$$

With the usual ansatz ${}_n \quad \mathrm{e}^{\mathrm{i}\omega n}\mathrm{e}^{\mathrm{i}}$ we find the dispersion relation in the form

$$2 \, (\cos \quad - 1) \quad 2(\cos\omega - 1) = 0, \tag{9}$$

where we a priori consider real values $0 \quad \omega, \quad 2$ due to periodicity of ${}_n$ and ${}_n$. Time reversal and spatial symmetry manifest themselves in the two cosine terms and allow a further reduction of the relevant interval to $0 \quad \omega, \quad .$

Relation (9) can be further analysed in two ways. If we study an initial-value problem, we should consider the wave number as real $0 \quad$ and analyse the frequency ω in dependence on and , . One can easily see that for $\frac{1}{4}$ and for each a real solution of ω exist. For $\frac{1}{4}$ a region of unstable perturbations with imaginary frequency ω appears.

If we study a boundary-value problem, we should consider real frequencies ω and look for corresponding solutions of . If a real solution exists, the boundary field with frequency ω produces a plane wave with the corresponding wave number. If there is no real solution of , the boundary field produces oscillations which are localized in space.

4. Qualitative description of periodic localized states

In our description of nonlinear localized states in the lattice we start from the so-called anti-continuous limit [15]. In this limit the coupling constant vanishes, so the mappings are independent. Thus, one simply chooses the initial

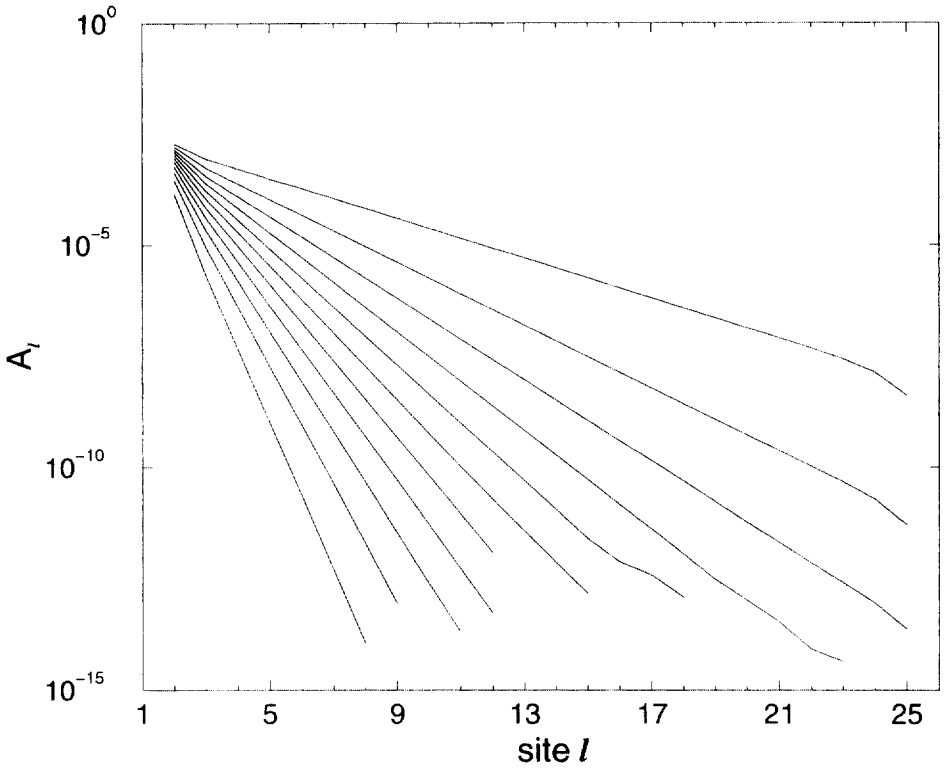

Fig. 2. Localized periodic orbits with rotation number $\frac{13}{21}$. The amplitude $= (1/\ )\sqrt{\sum_{n=1}\ _n{}^2}$ is plotted vs. the site for couplings $= 0.001, 0.002, \ , 0.011$ (from bottom to top).

conditions in such a way that for the first mapping $= 1$ the solution is a non-trivial periodic orbit (we denote its period by), and for all other mappings 1 the solution is the fixed point $= 0$, $=$. The idea is to continue this solution from $= 0$ to non-zero couplings (this continuation can be also done mathematically rigorous, see [2,14] for coupled differential equations and [41] for coupled maps). In the first approximation we can assume that the solution for small remains close to that for $= 0$, so it is close to the periodic orbit of the standard map for $= 1$ and to the stable fixed point for 1. Such a solution can be exact, if it does not radiate plane waves, i.e. if its frequencies lie outside the linear band.

In general, a periodic orbit of period has frequencies $\omega(\ , n) = n(2\ /\ )$, $n \in \mathbb{Z}$, where we consider only the components from 0 to $[\ /2 - 1]$ due to the above-mentioned symmetry arguments (here and hereafter $[\ ]$ denotes the integer part). For all of them we have to check if they belong to the linear band or not. The latter, according to the dispersion relation (9), includes frequencies $\omega_{\min} \ \omega \ \omega_{\max}$, where $\omega_{\max} = 2\arcsin \sqrt{/4}$ and $\omega_{\min} = 2\arcsin \sqrt{/4 -}$. The respective wave numbers are $(\omega_{\max}) = 0$ and $(\omega_{\min}) =$. Note first that the band width vanishes for $= 0$, so the perturbation with period leads to a localized state at least for small , provided that $n2\ /\ = \omega_{\max}$. Because only $\omega_{\min}$ depends on , the frequency component most dangerous from the point of view of localization is the one with

$$n = [\ \omega_{\max}/(2\ )] \tag{10}$$

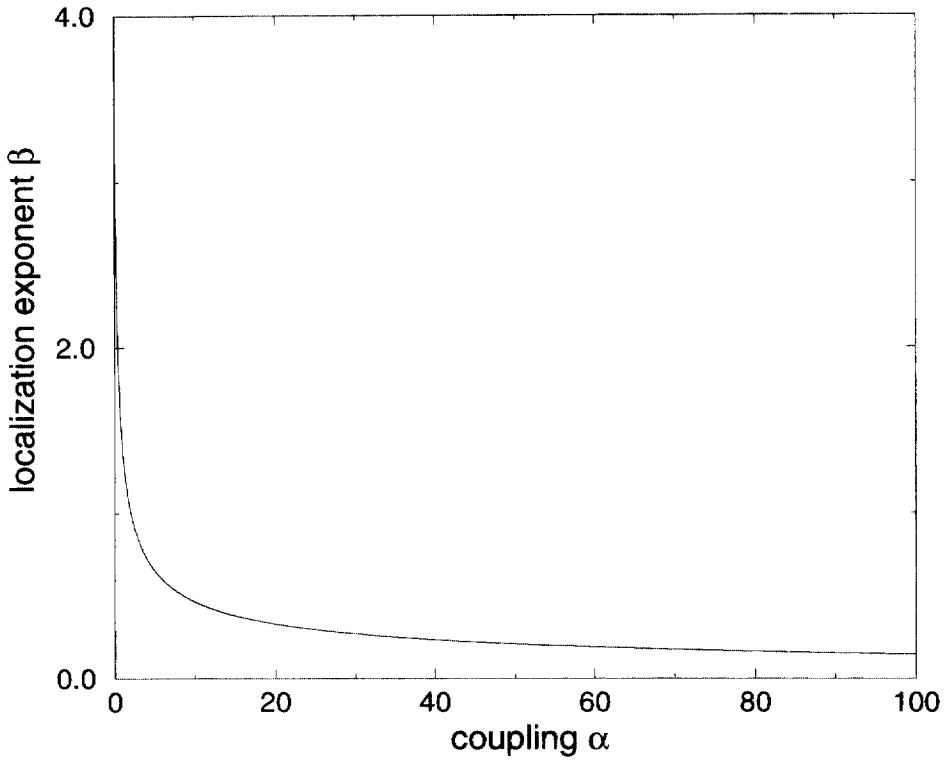

Fig. 3. Localization exponent β vs. coupling for the period-3 localized solution.

If $n^* = 0$, the localized solution continues to exist for all α. If $n^* > 0$, there exists a critical value of coupling α_{loc}, below which there is no localized state. This critical coupling satisfies

$$\alpha_{\mathrm{loc}} = K/4 - \sin^2\left(n^*\frac{\pi}{q}\right). \tag{11}$$

It is interesting to see, how the localization length of the solution changes with the parameter α. The asymptotic decay of the oscillations is given by the complex solution of the dispersion relation for $k = \pi + \mathrm{i}\beta$. Using (11) we obtain in some neighbourhood of α_{loc}

$$\cosh^2\left(\frac{\beta}{2}\right) = \alpha^{-1}\left(\frac{K}{4} - \sin^2\left(n^*\frac{\pi}{q}\right)\right) = \frac{\alpha_{\mathrm{loc}}}{\alpha}, \tag{12}$$

which relates the localization exponent β to the coupling constant α.

To clarify further this point we look at the spatial decay of the Fourier components of the breather. In order to do this, we use the method described in [11]. We write

$$\Theta_n^l = \sum_{m=1}^{q} \tilde{\Theta}_m^l \mathrm{e}^{\mathrm{i}mn\omega}$$

and get the Fourier transformed equations:

$$2\tilde{\Theta}_m^l(\cos(m\omega) - 1) = -K\tilde{\Theta}_m^l - K\tilde{F}_{1\,m}^l - \alpha(\tilde{\Theta}_m^{l+1} - 2\tilde{\Theta}_m^l + \tilde{\Theta}_m^{l-1}) - \alpha\tilde{F}_{2\,m}^l, \tag{13}$$

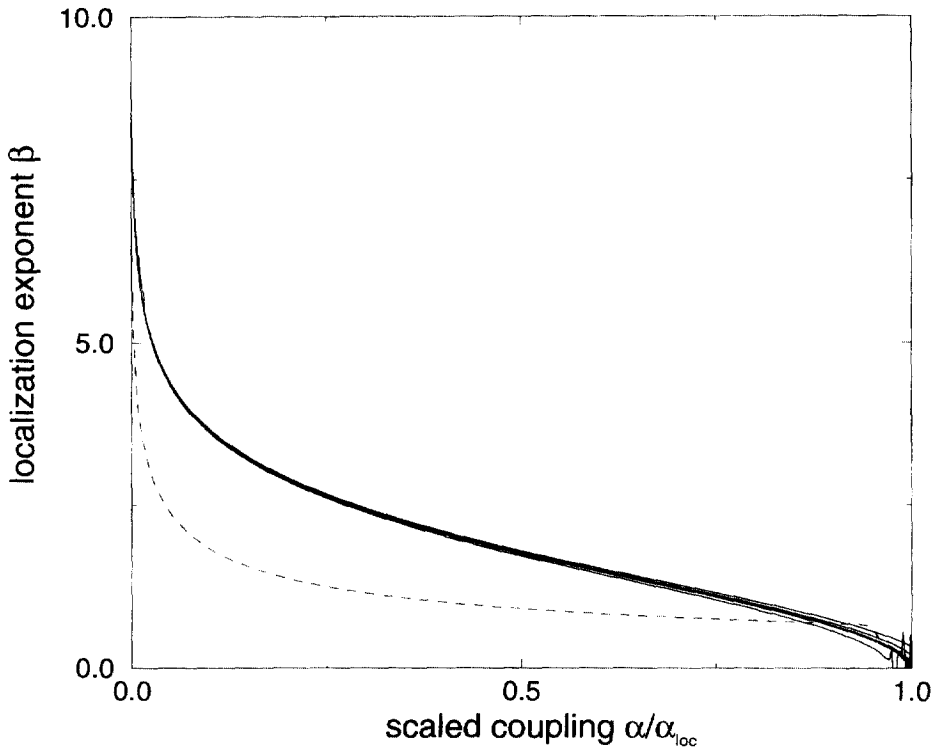

Fig. 4. Localization exponent vs. scaled coupling constant for the periodic orbits from $r = \frac{5}{8}$ to $r = \frac{89}{144}$, the graph from the linearized equation (12) coincides well and thus is hard to distinguish. The exponent for $\frac{8}{13}$ is shown as a dashed line.

where

$$\begin{aligned} F^l_{1\,m} &= \sin\Theta^l_n - \Theta^l_n, \\ F^l_{2\,m} &= \sin(\Theta^{l+1}_n - \Theta^l_n) - \sin(\Theta^l_n - \Theta^{l-1}_n) - (\Theta^{l+1}_m - 2\Theta^l_m + \Theta^{l-1}_m), \\ F^l_{1,2\,m} &= \sum_{m=1}^{q} \tilde{F}^l_{1,2\,m} \mathrm{e}^{\mathrm{i}mn\omega}. \end{aligned} \tag{14}$$

Each component $\tilde{\Theta}^l_m$ decays exponentially (without taking into account the nonlinear correction terms $\tilde{F}$) with a certain decay profile which depends on the parameter α (K is fixed). This is the generalization of Eq. (12) which relates only to the component closest to the band bottom. Depending on whether the component is above or below the band we have to use $\tilde{\Theta}^l_m \sim \mathrm{e}^{-\beta_m|l|}$ or $\tilde{\Theta}^l_m \sim \mathrm{e}^{\mathrm{i}\pi|l|-\beta_m|l|}$, respectively. With this we obtain

$$\cosh\beta_m = \frac{\pm 1}{\alpha}(\cos(m\omega) + K/2 - 1) + 1, \tag{15}$$

where the "−" is valid above and the "+" below the band. For each coupling we get a certain weakest decaying component $\tilde{\Theta}^l_m$. A special feature of the time discrete system is the symmetry of the modes which is expressed by the cosine term. We consider the right-hand side μ of (15) as a function of α:

$$\mu = \frac{1}{\omega}\arccos\left(\frac{2\alpha + 2 - K}{2}\right).$$

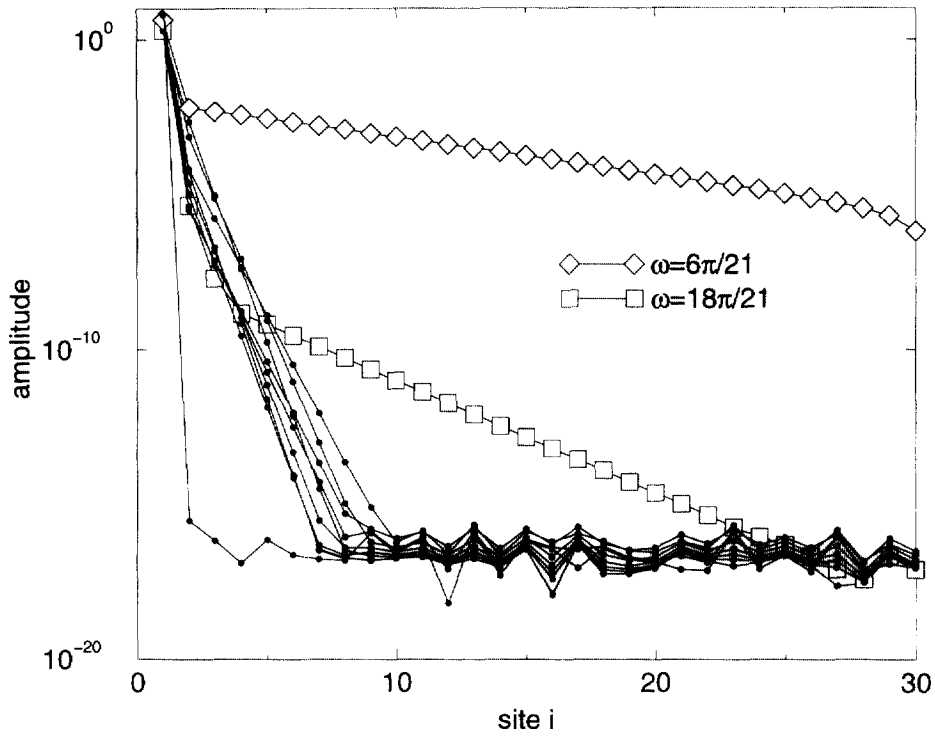

Fig. 5. Amplitude of all Fourier modes for the orbit with $r = \frac{13}{21}$, $\alpha = 0.01152$. Only the component next to the band bottom governs the decay, in this case the third harmonic with an exponent of $\beta_3 = 0.286$. The next more important component is the ninth harmonic whose weak decay ($\beta_9 = 0.827$) comes from correction terms due to nonlinear interaction with the third mode.

The governing component $\tilde{\Theta}^l_m$ is found as $[\mu + 1/2]$. At the anti-continuous limit, we can easily find the weakest decaying mode with $m = q \cdot [\arccos(0.6) + 1/2]$. With increasing coupling this may change, examples are described in Section 5.

It can happen that nonlinear terms in $\tilde{F}$ (see Eq. (13)) yield the leading order decay for modes other than the already discussed weakest decaying one [11]. This takes place whenever the frequency of the weakest decaying mode comes close enough to the band. Examples are discussed in the following section and are shown in the figures.

5. Localized periodic solutions – Numerical results

The qualitative consideration above suggests that periodic localized solutions in the coupled kicked rotators exist for some range of the coupling constant. To find these localized solutions numerically we start at the anti-continuous limit, i.e. with the zero coupling state where the first map moves on a periodic orbit and the rest is set to the period-1 fixed point $(J, \Theta) = (\pi, 0)$. We use a quasi-Newton method to find a periodic orbit in the whole lattice for non-vanishing coupling, and in order to get a continuous family of solutions we increase the coupling in small steps.

We investigate the localization properties of the chain. These are characterized by the localization exponent β or the localization length (which is simply the inverse of β). The exponent β is calculated from the slope of the spatial profile of the orbit in the linear region (large l).

A possible dependence on the chain length is investigated, such that we can be sure to use chains large enough to show the required effects, but not too large to avoid useless numerical efforts. In fact, we use a varying chain length,

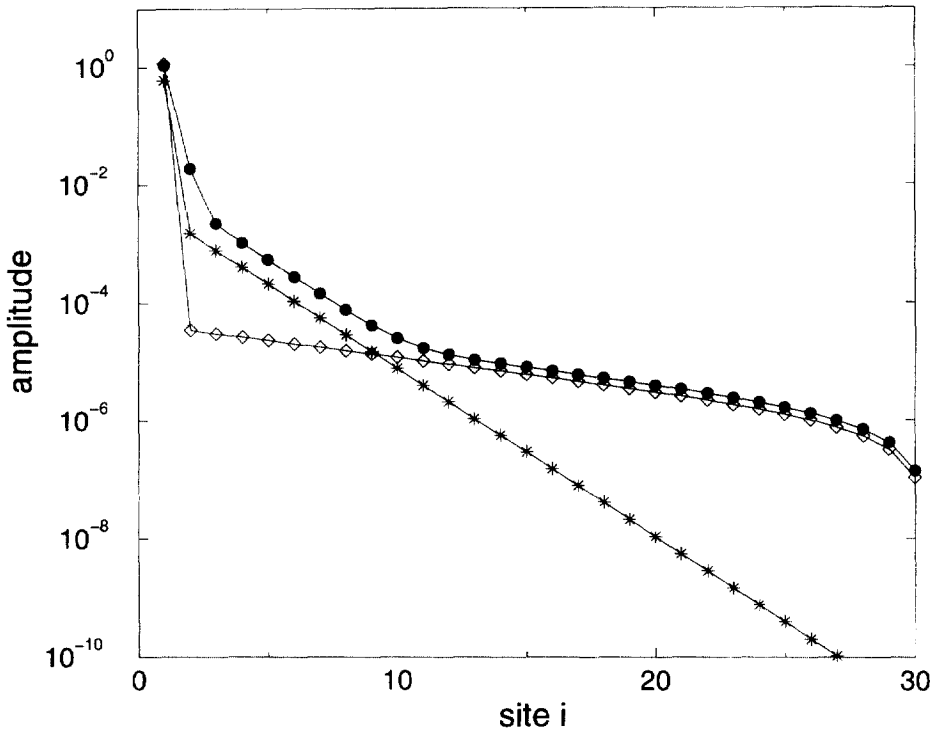

Fig. 6. Comparison of the decay of the first two Fourier components with the averaged action for the cycle with rotation number $\frac{8}{13}$ and coupling $\alpha = 0.1392$. The action is calculated as explained in Fig. 2 (filled circles). At the first sites the decay follows the second harmonic (stars); from site 11 on it is dominated by the first harmonic (diamonds).

where we start with 15 elements and prolongue the length automatically by units of two, if the last site comes in the range of the order of the numerical resolution.

To have a systematic approach to quasiperiodicity, we studied periodic regimes that approximate better and better the quasiperiodic state with the inverse golden mean rotation number [38,42,433]. [2] These periodic orbits have rotation numbers in the form F_n/F_{n+1} where F_n are the Fibonacci numbers. The advantage of using this special choice of periodic orbits is that in general it is not clear that high-period orbits exist at all (they can be eaten by the enlarged secondary stochastic regions) but they have been shown to exist in this case and these orbits are already used in some renormalization procedures considering the global stability of a single map [30,43]. Thus, if there is some systematic behaviour, the hope is that we can find it using this scheme.

To give an impression of the localized solution in the lattice, we display in Fig. 2 the logarithm of the time-averaged (over one period) amplitude A_l vs. site l. One can clearly see the localization down to the numerical resolution of 12 decimal digits. The slope of the graph allows us to determine the decay exponent β. The behaviour of the exponent with increasing coupling is displayed in Figs. 3 and 4.

We have found two scenarios of the evolution of periodic localized states as the coupling constant α increases (we remind that the nonlinearity parameter $K = 0.8$ remains constant). The first case holds for all periods $q < 6$, here the localized state exists for very large couplings $\alpha \gg 1$. The results are displayed in Fig. 3. The localization exponent shows a power-law dependence on the coupling. This behaviour is explained by the fact that for these

[2] We remind that for the standard map the rotation number is an average growth rate of the phase Θ, or, equivalently, the average of the action J.

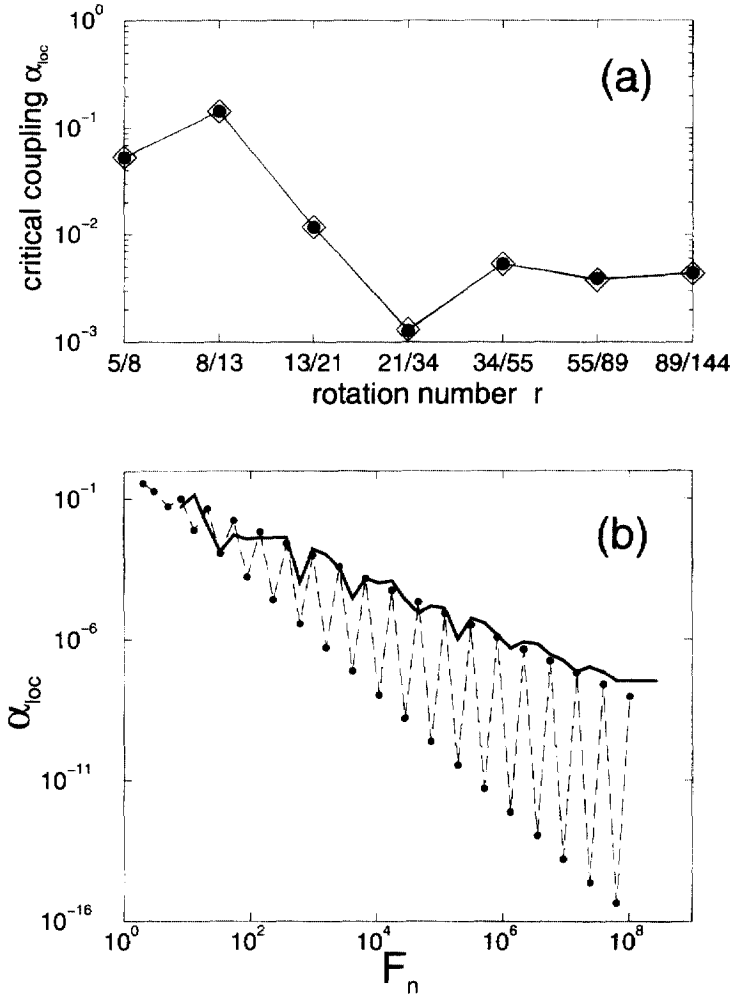

Fig. 7. (a) Critical couplings for localized solutions with different periods: numerically estimated (filled circles) and obtained from Eq. (11) (diamonds). (b) Solid line: the analytically obtained values for large values n of the Fibonacci numbers F_n corresponding to large periods q. Dashed line: the same for $\omega_{max} = 0.5(3\sqrt{5} - 5)$. The difference between the scaling for n odd and even can be clearly seen.

periods the value of n^* (Eq. (10)) is zero and the first harmonic of the spectrum lies above the linear band. Thus there cannot be any resonance of the periodic state with linear waves. Following the stability of the localized solution numerically, we have found that the first bifurcation that apppears is the instability of linear waves at $\alpha_c = \sqrt{K/4}$.

The second case holds for periodic orbits with periods larger than 6. Here the first harmonic lies below the linear band, and the localization gets lost according to the mechanism described in Section 4. The localization exponent β vanishes at the critical coupling α_{loc}, according to (11). The curves for β are in good agreement with the relation (12). In Fig. 4 the scaled graphs β vs. α/α_{loc} are shown and compared with the analytic result.

The rotation number $\frac{8}{13}$ seems to play a special role: there, the behaviour of the curves $\beta(\alpha)$ shows some overcross of the two scenarios described above. This happens because the second harmonic with $\omega = \frac{4}{13}\pi = 0.966$ is very close to the upper frequency of the band $\omega_{max} = 0.927$. Thus, this frequency dominates in the tail of the localized solution almost until the transition at α_{loc} where the first harmonic becomes the leading term in the tail.

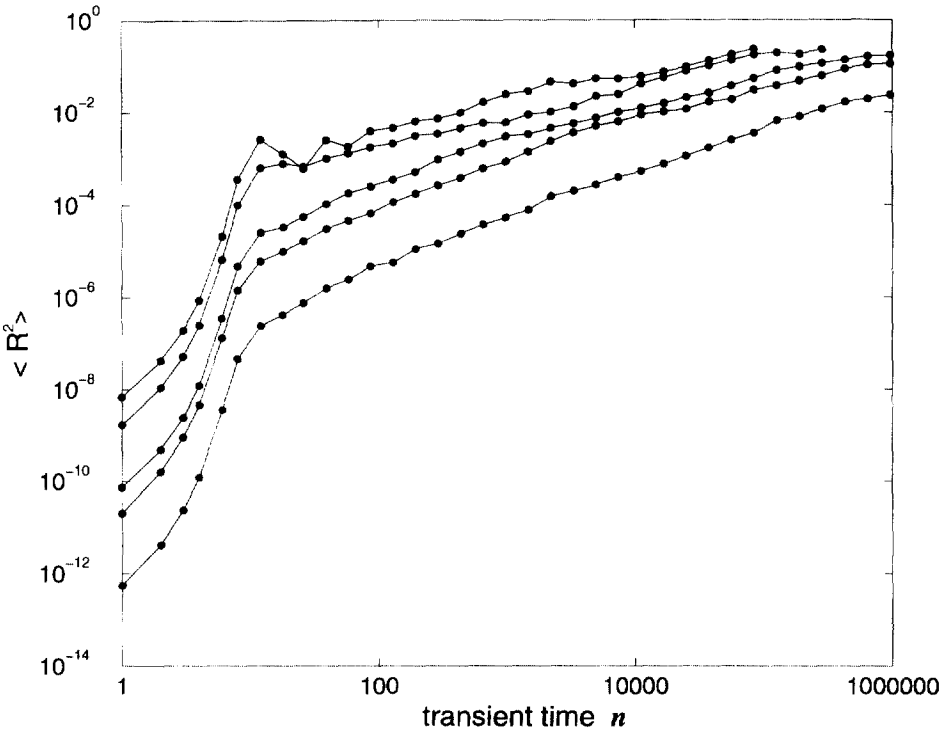

Fig. 8. Averaged radius in the second mapping $\langle R^2\rangle = 1/N \sum_{i=1}^{N} ((J_n^2)_i^2 + (\Theta_n^2)_i^2)$ of the distance to the period-1 fixed point vs. iteration time n (averaging over N initial conditions). From bottom to top, the couplings are $\alpha = 0.001, 0.005, 0.01, 0.05$ and 0.1. The diffusion constant is calculated from the slope of the graphs, for small enough coupling we get a value of $D \approx 1$.

The properties described above show up in the Fourier spectrum as an overcross from one decay component to another (Fig. 6). For small coupling, the second harmonic is closest to the band and thus governs the decay. For $\alpha = 0.029$ we get a very good agreement of the numerical value of $\beta_{2,\mathrm{num}} = 1.373598$, with the theoretical prediction $\beta_{2,\mathrm{theo}} = 1.373517$. With increasing coupling the influence of the first harmonic increases. For a coupling close to α_{loc}, one observes this transition as a steep decay in the first sites, coming from the influence of the second harmonic and a weaker decay in the mappings with higher site index from the first harmonic. Because we have two weak decaying modes at each side of the band whose nonlinear combinations influence all other modes, we have to include these higher corrections to calculate the correct decay in all the components.

As discussed in the previous section, we determined numerically for a stable period-21 solution the decay exponent for the two governing modes (Fig. 5). We compared the so-obtained values with the theoretical expectation from the linearized equation (15). For the coupling $\alpha = 0.01152$, the weakest decaying mode was the third harmonic where we found numerically an exponent of $\beta_{3,\mathrm{num}} = 0.286$ to be compared with the value $\beta_{3,\mathrm{theo}} = 0.278$ from Eq. (15). The second weakest-decaying component in the numerical result was the ninth with numerical and theoretical values of $\beta_{9,\mathrm{num}} = 0.827$ and $\beta_{9,\mathrm{theo}} = 5.555$, respectively. This is a perfect example for the case where nonlinear corrections (Eq. (14)) are important. In the tails (which means here $l > 5$) the dominating contribution is the weak decaying nonlinear correction term proportional to $(\tilde{\Theta}_3^l)^3$ which gives a correct exponent of $\beta_9 = 3 \cdot \beta_3 = 0.858$. The origin is the next higher contribution in the sine (cf. Eq. (14)), where the mixing of three modes with $m = 3$ gives the major contribution to the $m = 9$ mode (see also [11] for details).

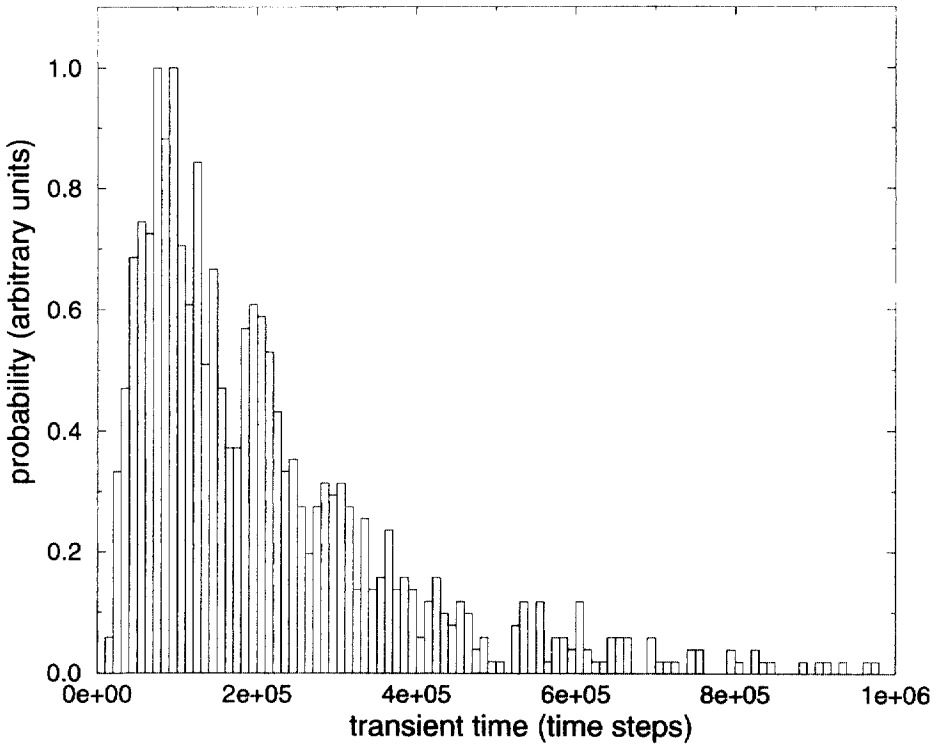

Fig. 9. Distribution of transient times to global chaos in a system of two coupled standard maps. An ensemble of 1000 initial conditions was chosen as described in the text.

With better and better approximation of the golden mean, we see that the periodic orbits get delocalized at smaller couplings for larger periods.

The values of α_{loc} demonstrate, however, no scaling as we are approaching the inverse golden mean. Indeeed, as one can see from (11), the values of α_{loc} are determined by the distance of a generally irrational number $2\arcsin\sqrt{K/4}$ to the closest number of the type $m2\pi/F_n$, and this distance decreases not regulary (see Figs. 7(a) and (b)). We can, however, roughly estimate $\alpha_{\mathrm{loc}} \sim F_n^{-1}$ because the distance between the harmonics is $2\pi/F_n$. This estimate is in good agreement with the data (Fig. 7(a)). One can expect a regularity in the behaviour of α_{loc} vs. n if the number $\omega_{\max} = 2\arcsin\sqrt{K/4}$ is regulary (self-similarly) approximated by the ratios of Fibonacci numbers (or, alternatively, if we choose periods according to denominators of the best continuous-fraction approximations of the number $\omega_{\max}$). To check this we choose the value of $\omega_{\max}$ to be a multiple of the golden mean. The continuous-fraction approximations based on the fractions with denominators F_n converge very fast (the error is $\sim (-1)^{n+1}F_n^{-2}$, this means that for n odd the approximation is from above, for n even it is from below). As in our case the spectrum of linear waves lies below $\omega_{\max}$, we get $\alpha_{\mathrm{loc},n} \sim F_n^{-2}$ for approximations with n even only (see Fig. 7(b)). For approximations with n odd, we have to take $(F_{n-1} - 1)/F_n$ instead of F_{n-1}/F_n, what immediately gives much worse convergence $\alpha_{\mathrm{loc},n} \sim F_n^{-1}$ seen in Fig. 7(b).

The results for the periodic localized states imply that time-quasiperiodic or time-chaotic localized states cannot exist generically. Indeed, a quasiperiodic orbit can be considered as a limit of a periodic orbit with period tending to infinity. The consideration above shows that in this limit the region of existence of a localized state vanishes. In the case of chaos, orbits with arbitrary large periods are embedded, therefore a localized state cannot exist as well. These considerations do not exclude that for special systems quasiperiodic states do exist as an exception.

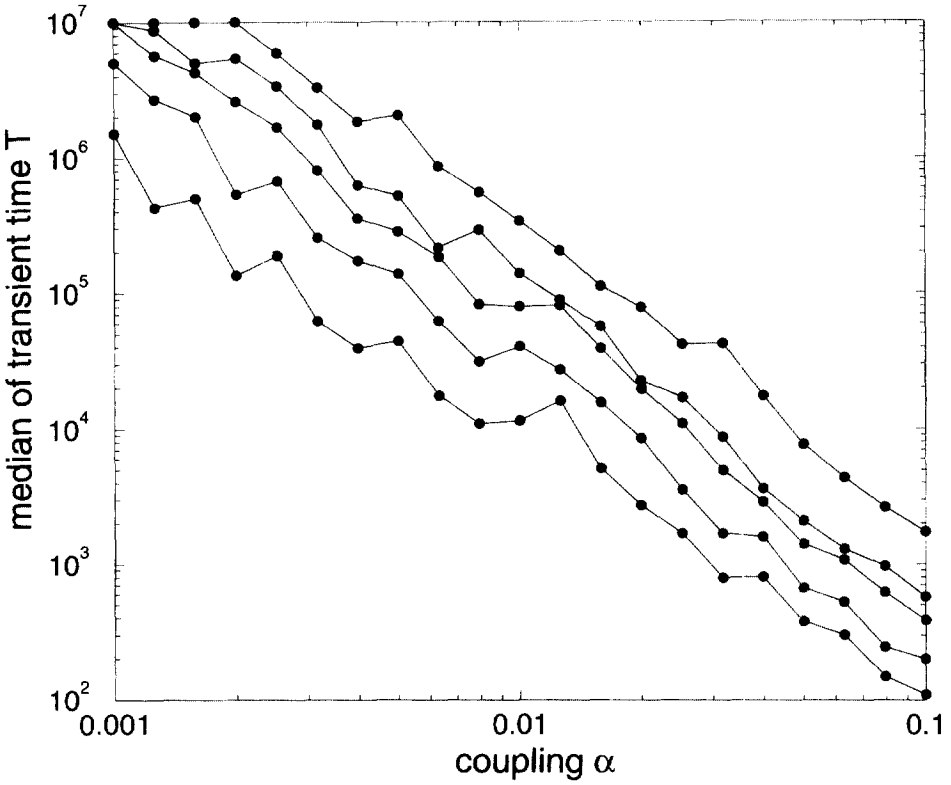

Fig. 10. Transient times T for onset of global chaos in the mappings in dependence on the coupling α. The graph displays the median of 25 different initial conditions for site 2,5,10, 15 and 20 (bottom to top), the chain length $L = 20$.

6. Time evolution of initially localized perturbations

The localized periodic state described above is a periodic orbit of a high-dimensional dynamical system. It can be realized if the initial conditions are prepared properly, but one can hardly expect to observe it for rather general initial conditions. Physically, it is interesting to know what happens to a localized initial state which is not an exact periodic solution of the full system. In this section we describe the evolution of the localized states for different initial conditions. We always choose the following initial configuration: all the oscillators are at the stable fixed point $J = 0$, $\Theta = \pi$, except for the first one. The coupling is non-zero with initialization. The initial state of the first oscillator was chosen in different regions of the phase space of the standard map (Fig. 1), correspondingly different dynamics in the lattice is observed.

There are two possibilities in interpretation of the results. From one side, decay of a breather can be described in terms of phonon radiation. From the other side, in the language of Hamiltonian systems one can refer also to Arnol'd diffusion [30] as the mechanism for the spreading of an initially localized object. It is important to clarify the connection between these two pictures.

In systems with three or more degrees of freedom, KAM surfaces do not isolate any longer the resonance layers of the system, rather these intersect and form a connected web, such that the trajectory can diffuse through the whole phase space. This net is called Arnol'd web, the according diffusion on this web Arnol'd diffusion (see [30] and references therein for details). We have here a special case of Arnol'd diffusion, as initially only one degree

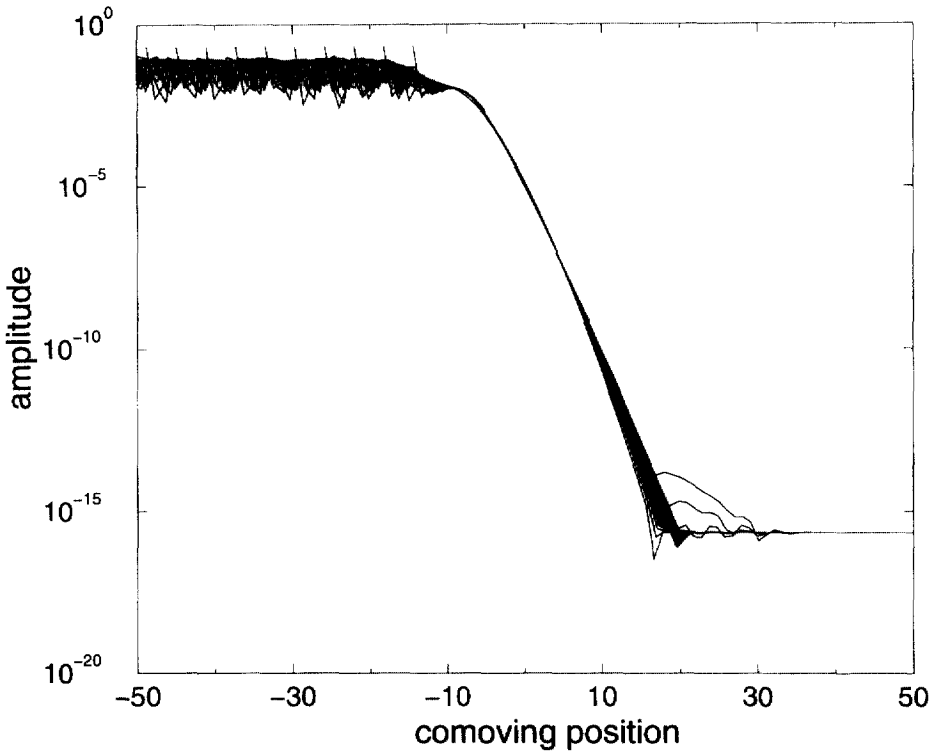

Fig. 11. Front profile for chaotic initial conditions, $\alpha = 0.001$ in a comoving frame. The profile decays exponentially in space, the front velocity is calculated to $v = 0.0019$ to be compared with the maximal group velocity of $v \approx 0.0013$.

of freedom is in a strongly nonlinear region of the phase space, while the rest of the lattice is in a nearly linear region. Thus, for initial stage of diffusion, when the perturbations in the lattice are small, the picture of phonon radiation is certainly correct. The higher the amplitudes of the radiated perturbaton, the less appropriate it is to use the phonon-based picture.

General properties of Arnol'd diffusion in the Hamiltonian lattices similar to that considered here have been discussed in [31–35]. Our case is specific as we consider the evolution of a specific spatial configuration. We distinguish two situations, initially locally chaotic and initially locally quasiperiodic states.

6.1. Chaotic initial local state

In order to place the first oscillator in the chaotic state, we used an initial point randomly chosen in a square $-0.001\pi < J^1 < 0.001\pi$, $-0.001\pi < \theta^1 < 0.001\pi$. If we let the system run after initialization, we observe first a propagation of disturbances into zero amplitude space with the velocity of this propagation corresponding to the velocity of linear waves in the lattice. As a result, a state with chaotic oscillations in the first element and non-zero but extremely small oscillating states in all other elements appears. Further evolution of the system is very slow [34,39]. Indeed, when a chaotic oscillator is coupled to non-chaotic ones, in the first approximation one can consider the latter ones as noise-driven with diffusive behaviour. In the lattice with nearest-neighbour coupling, the maximum diffusion is of course observed in the second oscillator, which is directly coupled to the chaotic one.

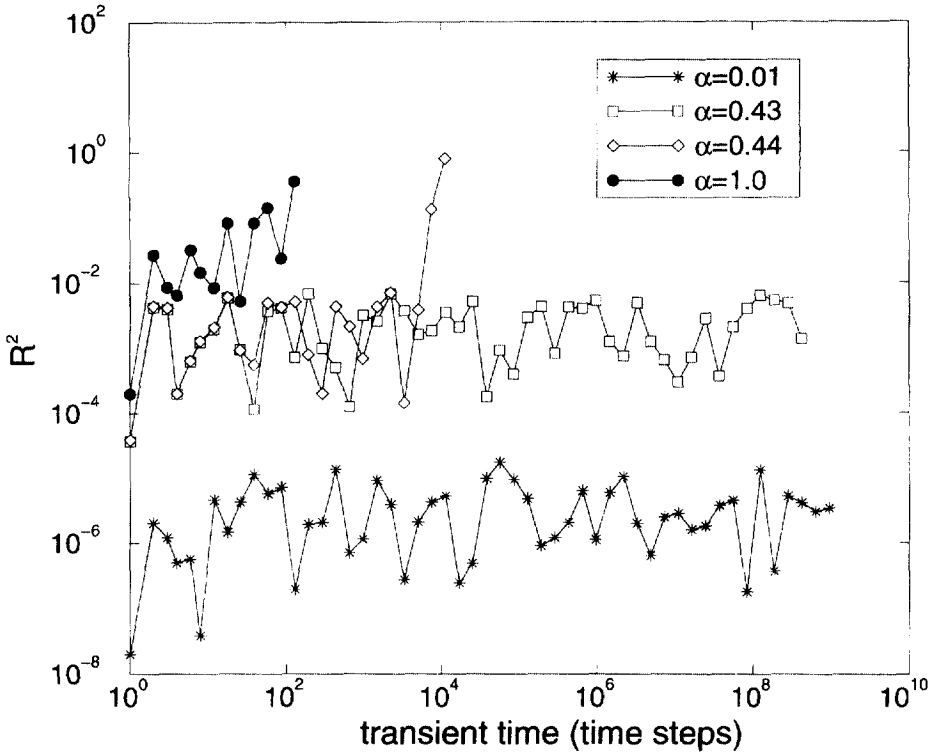

Fig. 12. Diffusion process in a chain of two mappings for only one initial condition ($J_0^1 = (\sqrt{5}-1)/2\pi$, $\Theta_0^1 = 0$, $J_0^2 = 0$, $\Theta_0^2 = \pi$) and various couplings (see legend). For couplings smaller than the critical one, here $\alpha = 0.44$, the regime in the second mapping stays bounded up to $T = 10^9$.

Thus, we follow [34] and consider first two coupled oscillators only. In the picture of the Arnol'd diffusion one has to look at the diffusion in the full, four-dimensional phase space. Since we are interested in the diffusion along the lattice, we look mainly at the projections onto the local subspaces, as proposed in [34,35]. In these papers, an analytic formula for thick and thin layer diffusion rates was obtained using a three resonances stochastic pump model and thus is valid for small excursions in the amplitude of the driven second mapping. This means, in particular, that small parameter values are required for the analytical model to hold, as already mentioned in [30,35]. The results are $D \sim \alpha^2 K \Theta_A^2$ for thick-layer diffusion (D is the diffusion coefficient, Θ_A the amplitude of the rotation in Θ_0) and $D \sim \alpha^2 \sqrt{K} \Theta_A^2$ for thin-layer diffusion. This has been already checked to be valid for small couplings and large enough times in the references mentioned above. We extend our considerations to large values of the coupling and try to describe the behaviour at small times, which was not mentioned in the previous works, but is important for the picture of phonon radiation. Furthermore, our actual goal is to investigate the diffusion along the spatial direction in a system with many mappings, which is discussed below.

For the situation of two mappings, we observe the following: while the first oscillator demonstrates chaos, the second one performs a random walk starting at the fixed point $J = 0$, $\Theta = \pi$. When the second oscillator reaches the stochastic layer, a global strong chaos is observed in both systems. This was determined by observation of the values of the action which extend then through the whole phase space.

An example for diffusion with different couplings is displayed in Fig. 8. The diffusion constant is estimated as the slope of the curve of the averaged square of the radius from the origin vs. the iteration time. At small

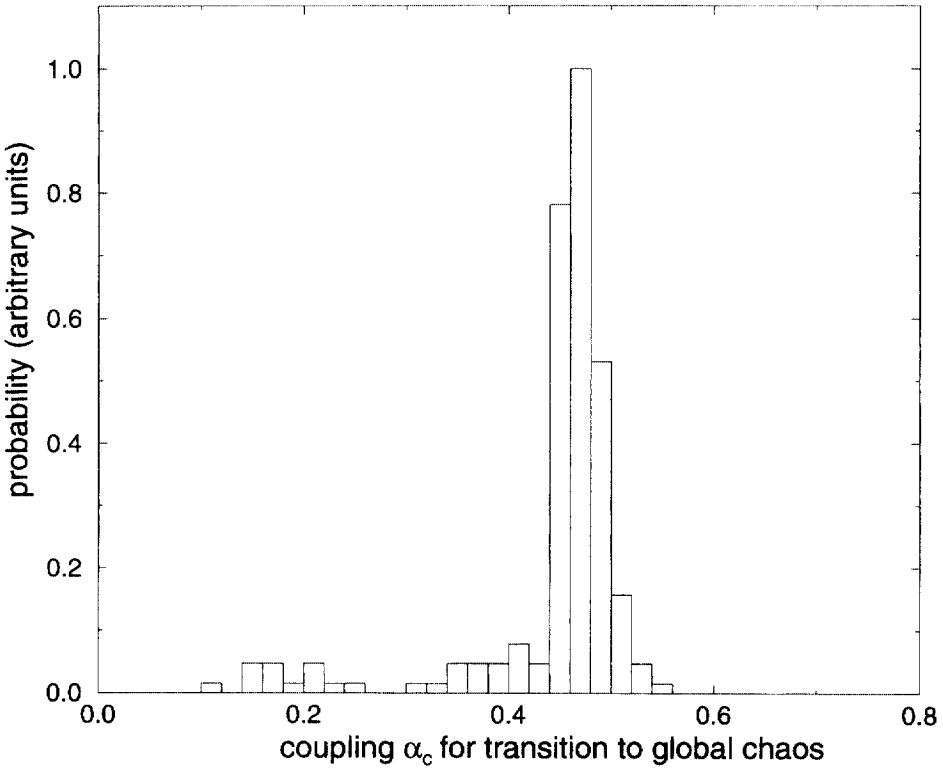

Fig. 13. Distribution of critical couplings for transition to global chaos for 200 different initial conditions chosen randomly around the golden mean rotational orbit. The most probable coupling is $\alpha = 0.47$.

times one can observe a fast increase due to the fast spread of linear perturbations. We get a diffusion constant $D = \Delta\langle R^2\rangle/\Delta T \approx 1$ for small couplings, for larger couplings the diffusion slows down slightly and does not follow any longer the analytic description.

The main characteristics of the process is the time of the random walk, i.e. the transient time before the global chaos sets in. In Fig. 9 we present a distribution of these times for an ensemble of different initial conditions in the first oscillator. One can see that for some orbits the transient time is extremely large. We attribute this to the intermittency that is typical for the Hamiltonian chaos: a trajectory can spend a long time in the nearly regular region at the border between chaos and quasiperiodicity [29,39]. Due to the appearance of large transient times, a suitable characteristic is the median of the distribution (Fig. 9); we plot this quantity (called transient time below) vs. coupling α in Fig. 10. In a large range of couplings the transient time obeys a power law $T \sim \alpha^{-1.46}$.

In the lattice of many coupled standard maps, the excitation of the third oscillator is enhanced when the global chaos in the first two oscillators appears, thus the transition time for it is only slightly larger than for the second oscillator. Further elements of the lattice reach the region of global chaos rather fast, see Fig. 10. As a result, a global fully developed chaotic state appears in the whole lattice.

The behaviour decsribed can be considered as an example of spatial development of chaos in Hamiltonian lattices. In the high-dimensional phase space it can be viewed as a motion on the Arnol'd web starting from rather exceptional initial conditions. As more and more oscillators reach the stochastic layer, they start to move in the major part of the available phase space and a statistically stationary regime sets in.

6.2. *Quasiperiodic initial local state*

To set the first map to a quasiperiodic state, we used initial conditions around the point $J^1 = \frac{1}{2}(\sqrt{5}-1)\pi$, $\Theta^1 = 0$ which is located on the KAM curve with the rotation number equal to the golden mean. As a first effect we observe the propagation of disturbances into the domain with zero amplitude, which happens with a constant velocity (see Fig. 11). For small couplings we find $v = 1.90\,\alpha$. This value has to be compared with the maximal group velocity of small perturbations according to the dispersion relation (9), where we calculate to first order in α $v = 1.25\,\alpha$.

After this initial stage a nearly localized state appears, where, however, the perturbation amplitude in the first oscillator is much larger than in the other ones. At this initial stage the dynamics is similar to that for a chaotic initial excitation. This is not surprising, because on small time scales there is no significant difference between chaotic and quasiperiodic motion.

We found the further evolution to depend significantly on the coupling α. For small couplings the nearly localized state remains localized even for very large times, up to 10^7, and is presumably stable (cf. Fig. 12). Contrary to this, for larger couplings we observe a slow growth of the amplitudes of oscillations at sites $l > 1$, so that eventually a regime of global chaos appears in the whole lattice. This was determined in the same way as above: when the trajectory reaches the primary stochastic region about the period one fixed point, the diffusion is driven fast and covers the whole $J_l - \Theta_l$ subspace. This transition in a system of two coupled maps is illustrated in Fig. 13, where the distribution of critical values of the coupling for transition to global chaos is depicted for 200 different initial conditions. The maximum of the distribution lies at $\alpha_c = 0.47$. In the system of several coupled maps qualitatively similar behaviour is observed, however the critical coupling decreases with the lattice length. This allows us to conclude that although we do not expect quasiperiodic breathers to exist, a quasiperiodic initial state may survive as a nearly localized extremely long living excitation.

7. Discussion and conclusion

In this paper we have considered localized excitations in a lattice of coupled standard maps. Localized periodic solutions can be found in analogy to breathers in continuous-time oscillator lattices. As the period grows (approaching a quasiperiodic state), the existence domain of breathers shrinks, which suggests that quasiperiodic localized states do not exist. However, we have found that for small couplings an initially localized quasiperiodic state survives in a nearly localized regime for very large times. If the coupling exceeds a critical value, slow excitation of neighbouring sites is observed, and eventually the lattice ends in a regime of global chaos. A chaotic initially localized state evolves similar: after a slow diffusion process, one by one the lattice sites reach the chaotic region.

The standard map considered throughout this paper is a typical nonlinear system, where regions of chaotic and quasiperiodic dynamics coexist. Thus, one can expect that properties of a lattice of standard maps represent typical behaviour of oscillator lattices, provided each oscillator is a high-dimensional system with more than one degree of freedom. Globally chaotic states are probably the most typical for such lattices, however a transient dynamics from initially localized excitations to this state may be very non-trivial.

Acknowledgements

We thank M. Spicci, R. Livi, M. Johansson, T. Cretegny, D. Bambusi for useful discussions. MA and AP acknowledge support by the Max-Planck foundation.

References

[1] R. Dodd, J. Eilbeck, J. Gibbon, H. Morris, Solitons and Nonlinear Wave Equations, Academic Press, London, 1982.
[2] S. Aubry, Physica D 103 (1997) 201.
[3] S. Flach, C. Willis, Phys. Rep. 295 (1998) 181.
[4] A.J. Sievers, S. Takeno, Phys. Rev. Lett. 61 (1988) 970.
[5] S. Takeno, J. Phys. Soc. Jpn. 59 (1990) 3861.
[6] S. Takeno, K. Hori, J. Phys. Soc. Jpn. 60 (1991) 947.
[7] S.R. Bickham, S.A. Kisilev, A.J. Sievers, Phys. Rev. B 47 (1993) 14206.
[8] S. Takeno, K. Kisoda, A.J. Sievers, Prog. Theor. Phys. Suppl. 94 (1988) 242.
[9] T. Dauxois, M. Peyrard, C.R. Willis, Physica D 57 (1992) 267.
[10] S. Flach, C.R. Willis, Phys. Lett. A 181 (1993) 232.
[11] S. Flach, Phys. Rev. E 51 (1995) 3579.
[12] S. Flach, Physica D 91 (1996) 223.
[13] S. Flach, K. Kladko, C.R. Willis, Phys. Rev. E 50 (1994) 2293.
[14] R.S. MacKay, S. Aubry, Nonlinearity 7 (1994) 1623.
[15] S. Aubry, G. Abramovici, Physica D 43 (1990) 199.
[16] K.W. Sandusky, J.B. Page, K.E. Schmidt, Phys. Rev. B 46 (1992) 6161.
[17] O.A. Chubykalo, A.S. Kovalev, O.V. Usatenko, Phys. Lett. A 178 (1993) 129.
[18] K.W. Sandusky, J.B. Page, Phys. Rev. B 50 (1994) 866.
[19] E.W. Laedke, K.H. Spatschek, S.K. Turitsyn, Phys. Rev. Lett. 73 (1994) 1055.
[20] T. Rössler, J.B. Page, Physica B 219–220 (1996) 387.
[21] J.B. Page, Physica B 219–220 (1996) 383.
[22] D. Bambusi, Nonlinearity 9 (1996) 433.
[23] R.S. MacKay, J.-A. Sepulchre, Physica D 119 (1998) 148.
[24] S. Flach, Phys. Rev. E 50 (1994) 3134.
[25] S. Flach, Phys. Rev. E 51 (1995) 1503.
[26] D. Cai, A.R. Bishop, N. Gronbech-Jensen, Phys. Rev. E 52 (1995) R5784.
[27] M. Johansson, S. Aubry, Yu.B. Gaididei, P.L. Christiansen, K.Ø. Rasmussen, Physica D 119 (1998) 115.
[28] C. Baesens, R. MacKay, private communication, 1997.
[29] B.V. Chirikov, Phys. Rep. 52 (1979) 265.
[30] A.J. Lichtenberg, M.A. Lieberman, Regular and Chaotic Dynamics, Springer, Berlin, 1992.
[31] K. Kaneko, R. Bagley, Phys. Lett. A 110 (1985) 435.
[32] T. Konishi, K. Kaneko, J. Phys. A 32 (1990) L715.
[33] K. Kaneko, T. Konishi, Phys. Rev. A 40 (1989) 40.
[34] B.P. Wood, A.J. Lichtenberg, M.A. Lieberman, Phys. Rev. A 42 (1990) 5885.
[35] G. Wang, B. Hu, Phys. Lett. A 151 (1990) 151.
[36] B.V. Chirikov, Phys. Rep. 52 (1979) 263.
[37] F.M. Russell, Y. Zzolotaryuk, J.C. Eilbeck, T. Dauxois, Preprint, 1996.
[38] L.M. Floria et al., Europhys. Lett. 36 (1996) 539.
[39] B.P. Wood,, A.J. Lichtenberg, M.A. Lieberman, Physica D 71 (1994) 132.
[40] G. Gyorgyi, F.M. Ling, G. Schmidt, Phys. Rev. A 40 (1989) 5311.
[41] M. Abel, M. Spicci, Physica D 119 (1998) 22.
[42] J.M. Greene, J. Math. Phys. 20 (1979) 760.
[43] R.S. MacKay, Physica D 7 (1983) 283.